Gravitoelectromagnetic coupled perturbations and quasinormal modes of a charged black hole with scalar hair

Wen-Di Guo, Qin Tan, and Yu-Xiao Liu*

Key Laboratory of Quantum Theory and Applications of MoE, Lanzhou Center for Theoretical Physics, Lanzhou University, Lanzhou 730000, China,
Key Laboratory of Theoretical Physics of Gansu Province, Institute of Theoretical Physics & Research Center of Gravitation, Lanzhou University, Lanzhou 730000, China,
and School of Physical Science and Technology, Lanzhou University, Lanzhou 730000, China

(Received 1 January 2023; revised 18 April 2023; accepted 30 May 2023; published 26 June 2023)

From the quantum point of view, singularity should not exist. Recently, Bah and Heidmann constructed a five-dimensional singularity free topology star/black hole [Phys. Rev. Lett. **126**, 151101 (2021)]. By integrating the extra dimension, a four-dimensional static spherically symmetric black hole with a magnetic charge and scalar hair can be obtained. In this paper, we study the quasinormal modes (QNMs) of the magnetic field and gravitational field on the background of this four-dimensional charged black hole with scalar hair. The odd parity of the gravitational perturbations couples with the even parity of the magnetic field perturbations. Two coupled second-order derivative equations are obtained. Using the matrix-valued direct integration method and the matrix-valued continued fraction method, we obtain the fundamental QNM frequencies numerically. The effect of the magnetic charge on the QNMs is studied. The differences of the frequencies of the fundamental QNMs between the charged black hole with scalar hair and the Reissner-Nordström black hole are very small for the angular number $l = 2$.

DOI: 10.1103/PhysRevD.107.124046

I. INTRODUCTION

Black hole physics has entered a new era since the detection of the gravitational waves from a binary black hole merger by Laser Interferometer Gravitational-Wave Observatory (LIGO) and Virgo [1] and the first picture of a supermassive black hole at the center of galaxy M87 photographed by the Event Horizon Telescope (EHT) [2–7]. Recently, the picture of the black hole in our Milky Way was also taken by EHT [8–13]. These breakthroughs provide us with more possibilities to test some fundamental physical problems, for example, the singularity problem in the mathematical aspect [14,15]. Usually, a spacetime singularity is located at the center of a black hole. However, from the quantum aspect, spacetime should not be singular. To mimic black holes classically, some ultracompact objects have been constructed, such as gravastars [16], boson stars [17], and wormholes [18–21]. For more details, see the review [22] and references therein. But usually they need some exotic matters, and the UV origin is unclear. From the top-down point of view, string theory is regarded as the candidate that can unify quantum theory and gravity. Some horizonless models constructed from string theory, such as fuzz balls [23], are similar to black holes up to the Planck scale, and they have smooth microstate geometries. However, a lot of degrees of freedom in supergravity are needed, and the astrophysical observations of these horizonless models are difficult [24–26]. Recently, a five-dimensional nonsingular topological star/black hole model was proposed based on a five-dimensional Einstein-Maxwell theory [27,28]. The spacetime in this model has advantages in both microstate (smooth geometry) and macrostate geometries (similar to classical black holes). So it is interesting to study their astrophysical observations. Last year, Lim studied the motion of a charged particle in this nonsingular topological star/black hole model [29]. The thermodynamic stability of the solutions has been carefully analyzed in Ref. [30]. Integrating the extra dimension, a four-dimensional Einstein-Maxwell-dilaton theory can be obtained, and a static spherically symmetric solution was solved in this background [25,26]. Shadows of this black hole were studied in Ref. [31]. In this paper, we will study the quasinormal modes (QNMs) of this model.

As the characteristic modes of a dissipative system, QNMs play important roles in a lot of aspects of our world. Because of the presence of the event horizon, black holes are natural dissipative systems. For a binary black hole merger system, there are three stages: inspiral, merger, and ringdown. In the ringdown stage, the gravitational waves are regarded as a superposition of QNMs [32]. Compared

*Corresponding author.
liuyx@lzu.edu.cn

with the normal modes, the eigenfunctions of QNMs generally do not form a complete set, and they are not normalizable [33]. The frequencies of QNMs are complex, and the imaginary parts are related to the decay timescale of the perturbation. One can use the QNMs to infer the mass and angular momentum of a black hole [34] and to test the validity of the no-hair theorem [35–37]. The echoes in the ringdown signals can be used to distinguish the black hole from the ultracompact objects [15,22,38]. Recently, the pseudospectrum of gravitational physics showed that the QNM spectrum is unstable for the fundamental mode and the overtone modes [39,40]. Besides, the properties of QNMs can also be used to constrain modified gravity theories [41–49]. The stability under perturbations of the background spacetime can also be partly revealed from the QNM frequencies [50,51]. Except for black hole physics, QNMs are also very useful in other dissipative systems, such as leaky resonant cavities [52] and brane world theories [53–55]. So, QNMs have been studied widely [56–60].

In this paper, we are interested in the QNMs of the four-dimensional spherically symmetric Bah-Heidmann black hole with a magnetic charge. The organization of this paper is as follows. In Sec. II, we briefly review the Bah-Heidmann black hole and the Kaluza-Klein (KK) reduction. In Sec. III, we study the linear perturbation of the electromagnetic field and gravitational field. Separating the radial part of the perturbed fields from the angular part, we derive the perturbation equations. In Sec. IV, we compute the quasinormal frequencies (QNFs) using the matrix-valued direct integration method. Finally, we give our conclusions in Sec. V.

II. THE CHARGED BLACK HOLE WITH SCALAR HAIR

In this section we briefly review the black hole/topological star model proposed by Bah and Heidmann [27,28]. We start from a five-dimensional Einstein-Maxwell theory. The action is

$$S = \int d^5x\sqrt{-\hat{g}}\left(\frac{1}{16\pi G_5}\hat{R} - \frac{1}{16\pi}\hat{F}^{MN}\hat{F}_{MN}\right), \quad (1)$$

where $\hat{F}_{MN}$ is the electromagnetic field tensor and G_5 is the five-dimensional gravitational constant. The quantities with a hat denote that they are constructed in the five-dimensional spacetime. The capital Latin letters $M, N, \ldots$ denote the five-dimensional coordinates. The metric can be assumed as [61]

$$ds^2 = -f_S(r)dt^2 + f_B(r)dy^2 + \frac{1}{f_S(r)f_B(r)}dr^2 + r^2d\theta^2 + r^2\sin^2\theta d\phi^2. \quad (2)$$

The extra dimension, denoted by the coordinate y, is a warped circle with radius R_y. The field strength with a magnetic flux is

$$\hat{F} = P\sin\theta d\theta\wedge d\phi. \quad (3)$$

The solution with double Wick rotation symmetry is [61]

$$f_B(r) = 1 - \frac{r_B}{r},$$
$$f_S(r) = 1 - \frac{r_S}{r},$$
$$P = \pm\frac{1}{G_5}\sqrt{3r_Sr_B}. \quad (4)$$

That is to say, the metric (2) is invariant under rotation $(t, y, r_S, r_B) \to (iy, it, r_B, r_S)$. There are two coordinate singularities located at $r = r_S$ (corresponding to a horizon) and $r = r_B$ (corresponding to a degeneracy of the y-circle). Bah and Heidmann found that, after some coordinate transformations, a smooth bubble locates at $r = r_B$ [27,28]. This provides an end of the spacetime. For $r_S \geq r_B$, the bubble is hidden behind the horizon and the metric (2) describes a black string. For $r_S < r_B$, the spacetime ends at the bubble before reaching the horizon, and the metric (2) describes a topological star [27,28].

We can integrate the extra dimension y (this process is called Kaluza-Klein reduction). Then, a four-dimensional Einstein-Maxwell-dilaton theory is obtained from the five-dimensional Einstein-Maxwell theory

$$S_4 = \int d^4x\sqrt{-g}\left(\frac{1}{16\pi G_4}R_4 - \frac{3}{8\pi G_4}g^{\mu\nu}\partial_\mu\Phi\partial_\nu\Phi - \frac{e^{-2\Phi}}{16\pi e^2}F_{\mu\nu}F^{\mu\nu}\right), \quad (5)$$

where $e^2 \equiv \frac{1}{2\pi R_y}$ and Φ is a dilaton field. The Greek letters $\mu, \nu, \ldots$, denote the four-dimensional coordinates. Here, $g_{\mu\nu}$ and $F_{\mu\nu}$ are the four-dimensional metric (15) and the electromagnetic field strength, respectively. The four-dimensional Ricci scalar R_4 is determined by the metric $g_{\mu\nu}$, and the four-dimensional gravitational constant is defined as

$$G_4 = e^2G_5. \quad (6)$$

Varying the action (5) with respect to the scalar field Φ, the vector potential A_μ, and the metric $g_{\mu\nu}$, we obtain the field equations

$$\frac{6}{G_4}\Box\Phi + \frac{e^{-2\Phi}}{e^2}F_{\mu\nu}F^{\mu\nu} = 0, \quad (7)$$

$$\nabla^\mu F_{\mu\nu} = 0, \quad (8)$$

$$R_{\mu\nu} - \frac{1}{2} g_{\mu\nu} = 8\pi G_4 T_{\mu\nu}, \tag{9}$$

where $\Box$ is the four-dimensional D'Alembert operator, $T_{\mu\nu} = T^{\rm s}_{\mu\nu} + T^{\rm m}_{\mu\nu}$ is the energy momentum tensor containing the contributions of the scalar field and the magnetic field:

$$T^{\rm s}_{\mu\nu} = \frac{3}{4\pi G_4} \nabla_\mu \Phi \nabla_\nu \Phi - \frac{3}{8\pi G_4} g_{\mu\nu} \Box \Phi, \tag{10}$$

$$T^{\rm m}_{\mu\nu} = \frac{e^{-2\Phi}}{4\pi e^2} F_{\mu\alpha} F^\alpha_\nu - \frac{e^{-2\Phi}}{16\pi e^2} g_{\mu\nu} F_{\alpha\beta} F^{\alpha\beta}. \tag{11}$$

The dilaton field Φ can be obtained as

$$e^{2\Phi} = f_B^{-1/2}. \tag{12}$$

We can solve the vector potential corresponding to the magnetic field as

$$A_\mu = \left(0, 0, 0, -\frac{e}{2}\sqrt{\frac{3 r_B r_S}{G_4}} \cos\theta\right). \tag{13}$$

Thus, the field strength reads as

$$F_{\mu\nu} = \begin{bmatrix} 0 & 0 & 0 & 0 \\ 0 & 0 & 0 & 0 \\ 0 & 0 & 0 & \frac{e}{2}\sqrt{\frac{3 r_B r_S}{G_4}} \sin\theta \\ 0 & 0 & -\frac{e}{2}\sqrt{\frac{3 r_B r_S}{G_4}} \sin\theta & 0 \end{bmatrix}. \tag{14}$$

The four-dimensional metric is

$$ds_4^2 = f_B^{\frac{1}{2}} \left(-f_S dt^2 + \frac{dr^2}{f_B f_S} + r^2 d\theta^2 + r^2 \sin^2\theta d\phi^2\right). \tag{15}$$

Note that, when $r_B = 0$, this metric recovers to the Schwarzschild one.

The parameters r_S and r_B are related to the four-dimensional Arnowitt-Deser-Misner mass M and the magnetic charge $Q_{\rm m}$ as

$$M = \left(\frac{2 r_S + r_B}{4 G_4}\right), \tag{16}$$

$$Q_{\rm m} = \frac{1}{2}\sqrt{\frac{3 r_B r_S}{G_4}}. \tag{17}$$

On the other hand, for each M and $Q_{\rm m}$, which are physical parameters, there are two solutions of (r_S, r_B),

$$r_S^{(1)} = 2G_4(M - M_\triangle), \qquad r_B^{(1q)} = G_4(M + M_\triangle); \tag{18}$$

$$r_S^{(2)} = G_4(M + M_\triangle), \qquad r_B^{(2)} = 2G_4(M - M_\triangle), \tag{19}$$

where

$$M_\triangle^2 = M^2 - \left(\frac{\sqrt{2} Q_{\rm m}}{\sqrt{3 G_4}}\right)^2. \tag{20}$$

Note that, in four-dimensional spacetime, when $r < r_B$, $f_B^{1/2}$ becomes imaginary. So, $r = r_B$ is the end of the spacetime. This is consistent with the result in five-dimensional spacetime [27,28]. Usually, a black string scenario has the Gregory-Laflamme instability [62]. However, compact extra dimensions leading to a discrete KK mass spectrum make it possible to avoid the Gregory-Laflamme instability. Stotyn and Mann demonstrated that the solution (18) is unstable under perturbation, while, when $R_y > \frac{4\sqrt{3}}{3} Q_{\rm m}$, the solution (19) is stable. That is to say, the solution (19) does not have the Gregory-Laflamme instability. Actually, the spacetime at $r = r_B$ is singular in four-dimensional spacetime. When $r_B \geq r_S$, the metric (15) corresponds to a naked singularity, and when $r_B < r_S$, the metric (15) corresponds to a black hole, which is named as a charged black hole with scalar hair. In this paper, we will only focus on the case $r_B < r_S$, i.e., the charged black hole with scalar hair.

III. PERTURBATION EQUATIONS

With the background solution (12), (15), and (13), we can derive the equations of motion for the perturbations. The perturbed scalar field, vector potential, and metric field can be written as

$$\Phi = \bar{\Phi} + \varphi, \tag{21}$$

$$A_\mu = \bar{A}_\mu + a_\mu, \tag{22}$$

$$g_{\mu\nu} = \bar{g}_{\mu\nu} + h_{\mu\nu}, \tag{23}$$

where the quantities with a bar represent the background fields and φ, a_μ, and $h_{\mu\nu}$ denote the corresponding perturbations. Because the background spacetime is spherically symmetric, the perturbations can be divided into three parts based on their transformations under rotations on the two-sphere: scalars, two-dimensional vectors, and two-dimensional tensors. The spherical harmonic function $Y_{l,m}(\theta, \phi)$ behaves as a scalar under rotations, so it is the scalar base. The two-dimensional vector and tensor bases are introduced as follows [63–67]:

$$(V^1_{l,m})_a = \partial_a Y_{l,m}(\theta, \phi), \tag{24}$$

$$(V^2_{l,m})_a = \gamma^{bc} \epsilon_{ac} \partial_b Y_{l,m}(\theta, \phi), \tag{25}$$

for the vector part, and

$$(T^1_{l,m})_{ab} = (Y_{l,m})_{;ab}, \tag{26}$$

$$(T^2_{l,m})_{ab} = Y_{l,m}\gamma_{ab}, \tag{27}$$

$$(T^3_{l,m})_{ab} = \frac{1}{2}[\epsilon^c_a(Y_{l,m})_{;cb} + \epsilon^c_b(Y_{l,m})_{;ca}], \tag{28}$$

for the tensor part. Here, the Latin letters a, b, c denote the angular coordinates θ and ϕ, γ is the induced metric on the two-sphere with radius 1, and ϵ is the totally antisymmetric tensor in two dimensions. The semicolon denotes the covariant derivative on the two-sphere.

The above quantities behave differently under the space inversion, i.e., $(\theta,\phi) \to (\pi-\theta, \pi+\phi)$. A quantity is called even or polar if it acquires a factor of $(-1)^l$ under space inversion. A quantity is called odd or axial if it acquires a factor of $(-1)^{l+1}$ under space inversion. So the above quantities can be divided into two classes, the even parts $V^1_{l,m}, T^1_{l,m}, T^2_{l,m}$, and the odd parts $V^2_{l,m}, T^3_{l,m}$. Note that, the spherical harmonic function $Y_{l,m}(\theta,\phi)$ is even parity. Usually the gravitational and electromagnetic perturbations will mix, for example, the Reissner-Nordström (RN) black hole. But the even-parity and odd-parity perturbations usually do not mix, the RN black hole with electric charge does not mix the polar and axial contributions. Only the even-parity (or odd-parity) perturbations of the gravitational and electromagnetic parts mix. However, we can see from Eqs. (12), (15), and (13) that the background scalar field and metric field are even parity and the background vector potential is odd parity. So we expect that the scalar perturbation and even-parity parts of the metric perturbations couple to the odd-parity parts of the electromagnetic perturbations to the linear order (type-I coupling). And the odd-parity parts of the metric perturbations couple to the even-parity parts of the electromagnetic perturbations to the linear order (type-II coupling). Note that the scalar perturbation only contains the even part. Actually, these coupled perturbation equations have been studied in Refs. [68,69]. In this paper, we study the type-II coupling perturbations.

Based on the principle of general covariance, the theory should keep covariant under an infinitesimal coordinate transformation. Thus, we can choose a specific gauge to simplify the problem. In the Regge-Wheeler gauge [66], the odd parts of the perturbation $h_{\mu\nu}$ can be written as

$$h_{\mu\nu} = \sum_l e^{-i\omega t}\begin{bmatrix} 0 & 0 & 0 & h_0 \\ 0 & 0 & 0 & h_1 \\ 0 & 0 & 0 & 0 \\ * & * & 0 & 0 \end{bmatrix} \sin\theta\partial_\theta Y_{l,0}(\theta). \tag{29}$$

The magnetic field also has a gauge freedom. Following Ref. [70], we denote

$$\tilde{f}_{\mu\nu} = \partial_\mu a_\nu - \partial_\nu a_\mu, \tag{30}$$

and the even parts of the perturbation $\tilde{f}_{\mu\nu}$ can be written as

$$\tilde{f}_{\mu\nu} = \sum_l e^{-i\omega t}\begin{bmatrix} 0 & f_{01} & f_{02} & 0 \\ * & 0 & f_{12} & 0 \\ 0 & * & 0 & 0 \\ 0 & * & 0 & 0 \end{bmatrix} \sin\theta\partial_\theta Y_{l,0}(\theta). \tag{31}$$

Note that we have chosen $m = 0$ for simplicity, because the perturbation equations do not depend on the value of m [66]. The asterisks denote elements obtained by symmetry. The functions h_0, h_1, f_{01}, f_{02}, and f_{12} only depend on the coordinate r. The perturbation of the vector potential can be expanded as

$$a_t = -\sum_l e^{-i\omega t} f_{02} Y_{l,0}, \tag{32}$$

$$a_r = -\sum_l e^{-i\omega t} f_{12} Y_{l,0}, \tag{33}$$

$$a_\theta = 0, \tag{34}$$

$$a_\phi = 0. \tag{35}$$

The field strength f_{01} can be derived from Eq. (30) as

$$f_{01} = \partial_r f_{02} + i\omega f_{12}. \tag{36}$$

Substituting Eqs. (29) and (31) into the equations of motion (8) and (9), after some algebra calculations we can obtain the following master perturbation equations:

$$\frac{d^2\psi_{\rm g}}{dr_*^2} + (\omega^2 - V_{11})\psi_{\rm g} - V_{12}\psi_{\rm m} = 0, \tag{37}$$

$$\frac{d^2\psi_{\rm m}}{dr_*^2} + (\omega^2 - V_{22})\psi_{\rm m} - V_{21}\psi_{\rm g} = 0, \tag{38}$$

where

$$\psi_{\rm g} \equiv f_B^{1/4} f_S \frac{1}{r} h_1, \tag{39}$$

$$\psi_{\rm m} \equiv \sqrt{f_B} r^2 f_{01}, \tag{40}$$

r_* is the tortoise coordinate defined as

$$dr_* = \frac{1}{\sqrt{f_B f_S}} dr, \tag{41}$$

and

$$V_{11} = f_S\left[\frac{l(l+1)}{r^2} - \frac{3(r_B^2(13r_S - 9r) + 16r_S r^2)}{16 f_B r^5}\right] + f_S\frac{3r_B(2r - 7r_S)}{4f_B r^4}, \tag{42}$$

$$V_{12} = -\frac{2if_S f_B^{1/4}}{el(l+1)r^3}\sqrt{3r_B r_S G_4}\omega, \tag{43}$$

$$V_{21} = \frac{i\sqrt{3r_B r_S}ef_S}{2\sqrt{G_4}\omega f_B^{1/4}r^3}(l-1)l(l+1)(l+2), \tag{44}$$

$$V_{22} = f_S\left[\frac{3r_B r_S}{r^4} + \frac{l(l+1)}{r^2}\right]. \tag{45}$$

The details of deriving the master equations (37) and (38) are shown in Appendix.

Note that, when the magnetic charge $Q_{\rm m}$ vanishes, or r_B approaches zero, the gravitational perturbation $\psi_{\rm g}$ and the magnetic field perturbation $\psi_{\rm m}$ will decouple. Furthermore, the potential V_{11} will reduce to the potential for the gravitational perturbation of the Schwarzschild black hole. Besides, the parameters e and G_4 do not affect the quasinormal modes. To see this, we can redefine

$$\tilde{\psi}_{\rm m} \equiv \frac{\sqrt{G_4}}{e}\psi_{\rm m} \tag{46}$$

to eliminate the parameters e and G_4 in Eqs. (37) and (38). The corresponding potentials are

$$\tilde{V}_{12} = -\frac{2if_S f_B^{1/4}}{l(l+1)r^3}\sqrt{3r_B r_S}\omega, \tag{47}$$

$$\tilde{V}_{21} = \frac{i\sqrt{3r_B r_S}f_S}{2\omega f_B^{1/4}r^3}(l-1)l(l+1)(l+2). \tag{48}$$

In the following, we use the redefined quantities but omit the tilde above them.

IV. QUASINORMAL MODES

In this section we will solve the master perturbation equations (37) and (38) to obtain the frequencies of the QNMs. We focus on the QNMs of the solution (19) because it is free of the Gregory-Laflamme instability. We know from Eq. (20) that the range of the magnetic charge $Q_{\rm m}$ is $[0, \sqrt{\frac{3}{2}G_4}M]$. Compared with the range of the electric charge of the RN black hole $[0, \sqrt{G_4}M]$, the range of the magnetic charge is larger than that of the RN black hole electric charge. Note that we only study the charged black hole with scalar hair, that is, $r_B < r_S$. In this situation, the range of the magnetic charge $Q_{\rm m}$ is $[0, 2\sqrt{\frac{G_4}{3}}M]$. This range is still larger than that of the RN black hole electric charge.

The perturbation equations (37) and (38) are coupled and can be rewritten into a compact form

$$\frac{d^2\mathbf{Y}}{dr_*^2} + (\omega^2 - \mathbf{V})\mathbf{Y} = 0, \tag{49}$$

where

$$\mathbf{Y} = \begin{pmatrix}\psi_{\rm g}\\ \psi_{\rm m}\end{pmatrix}$$

and $\mathbf{V}$ is a 2×2 matrix with components (42), (45), (47), and (48). The physical boundary conditions for the QNM problem are pure ingoing waves at the event horizon

$$Y_n \sim b_n e^{-i\omega r_*}, \qquad r_* \to -\infty, \tag{50}$$

and pure outgoing waves at spatial infinity

$$Y_n \sim B_n e^{i\omega r_*}, \qquad r_* \to +\infty, \tag{51}$$

where Y_n is the nth component of $\mathbf{Y}$, and b_n and B_n are coefficients of the boundary conditions. With these boundary conditions, solving the QNFs is an eigenvalue problem.

The continued fraction method was first applied to gravitational problems by Leaver [71], and it has been used in a coupled system [72,73]. To get a recurrence relation, we need a suitable ansatz of the eigenfunction. Here, we assume that eigenfunctions of $\psi_{\rm g}$ and $\psi_{\rm m}$ are

$$\psi_{\rm g} = (r-r_S)^{-p}(r-r_S+1)^p e^{i(r-r_S)\omega}(r-r_S+1)^{i(r_B/2+r_S)\omega}\sum_n a_n^g H(r)^n, \tag{52}$$

$$\psi_{\rm m} = (r-r_S)^{-p}(r-r_S+1)^p e^{i(r-r_S)\omega}(r-r_S+1)^{i(r_B/2+r_S)\omega} f_B(r)^{3/4}\sum_n a_n^m H(r)^n, \tag{53}$$

where $p = \frac{ir_S^{3/2}\omega}{\sqrt{r_s - r_B}}$ and $H(r) = \frac{r-r_S}{r-r_B}$. Inserting these into the master equations (37) and (38), we obtain seven-term recurrence relations

$$\alpha_0 \mathbf{A_1} + \beta_0 \mathbf{A_0} = 0, \tag{54}$$

$$\alpha_1 \mathbf{A_2} + \beta_1 \mathbf{A_1} + \gamma_1 \mathbf{A_0} = 0, \tag{55}$$

$$\alpha_2 \mathbf{A_3} + \beta_2 \mathbf{A_2} + \gamma_2 \mathbf{A_1} + \rho_2 \mathbf{A_0} = 0, \tag{56}$$

$$\alpha_3 \mathbf{A_4} + \beta_3 \mathbf{A_3} + \gamma_3 \mathbf{A_2} + \rho_3 \mathbf{A_1} + \lambda_3 \mathbf{A_0} = 0, \tag{57}$$

$$\alpha_4 \mathbf{A_5} + \beta_4 \mathbf{A_4} + \gamma_4 \mathbf{A_3} + \rho_4 \mathbf{A_2} + \lambda_4 \mathbf{A_1} + \sigma_4 \mathbf{A_0} = 0, \tag{58}$$

$$\alpha_\mathbf{n} \mathbf{A_{n+1}} + \beta_\mathbf{n} \mathbf{A_n} + \gamma_\mathbf{n} \mathbf{A_{n-1}} + \rho_\mathbf{n} \mathbf{A_{n-2}} + \lambda_\mathbf{n} \mathbf{A_{n-3}} + \sigma_\mathbf{n} \mathbf{A_{n-4}} + \delta_\mathbf{n} \mathbf{A_{n-5}} = 0, \tag{59}$$

where

$$\mathbf{A_n} = \begin{pmatrix} a_n^g \\ a_n^m \end{pmatrix}$$

is the vectorial coefficient. The coefficient matrices of the recurrence relations are very complicated, so we do not show the explicit expressions [74]. Usually, a three-term recurrence relation can be obtained through a matrix-valued version of the Gaussian elimination [75,76]. Then a matrix-valued continued fraction can be solved and can be used to solve the QNFs. More details can be seen in Ref. [77]. However, it needs to solve the inverse of the coefficient matrices of the recurrence relations again and again, which is difficult. There is an equivalent way to solve the QNFs. Equations (54)–(59) can be written as

$$\begin{pmatrix}
\beta_0^{11} & \beta_0^{12} & \alpha_0^{11} & \alpha_0^{12} & & & & & & & & & & & & \\
\beta_0^{21} & \beta_0^{22} & \alpha_0^{21} & \alpha_0^{22} & & & & & & & & & & & & \\
\gamma_1^{11} & \gamma_1^{12} & \beta_1^{11} & \beta_1^{12} & \alpha_1^{11} & \alpha_1^{12} & & & & & & & & & & \\
\gamma_1^{21} & \gamma_1^{22} & \beta_1^{21} & \beta_1^{22} & \alpha_1^{21} & \alpha_1^{22} & & & & & & & & & & \\
\rho_2^{11} & \rho_2^{12} & \gamma_2^{11} & \gamma_2^{12} & \beta_2^{11} & \beta_2^{12} & \alpha_2^{11} & \alpha_2^{12} & & & & & & & & \\
\rho_2^{21} & \rho_2^{22} & \gamma_2^{21} & \gamma_2^{22} & \beta_2^{21} & \beta_2^{22} & \alpha_2^{21} & \alpha_2^{22} & & & & & & & & \\
\lambda_3^{11} & \lambda_3^{12} & \rho_3^{11} & \rho_3^{12} & \gamma_3^{11} & \gamma_3^{12} & \beta_3^{11} & \beta_3^{12} & \alpha_3^{11} & \alpha_3^{12} & & & & & & \\
\lambda_3^{21} & \lambda_3^{22} & \rho_3^{21} & \rho_3^{22} & \gamma_3^{21} & \gamma_3^{22} & \beta_3^{21} & \beta_3^{22} & \alpha_3^{21} & \alpha_3^{22} & & & & & & \\
\sigma_4^{11} & \sigma_4^{12} & \lambda_4^{11} & \lambda_4^{12} & \rho_4^{11} & \rho_4^{12} & \gamma_4^{11} & \gamma_4^{12} & \beta_4^{11} & \beta_4^{12} & \alpha_4^{11} & \alpha_4^{12} & & & & \\
\sigma_4^{21} & \sigma_4^{22} & \lambda_4^{21} & \lambda_4^{22} & \rho_4^{21} & \rho_4^{22} & \gamma_4^{21} & \gamma_4^{22} & \beta_4^{21} & \beta_4^{22} & \alpha_4^{21} & \alpha_4^{22} & & & & \\
\delta_5^{11} & \delta_5^{12} & \sigma_5^{11} & \sigma_5^{12} & \lambda_5^{11} & \lambda_5^{12} & \rho_5^{11} & \rho_5^{12} & \gamma_5^{11} & \gamma_5^{12} & \beta_5^{11} & \beta_5^{12} & \alpha_5^{11} & \alpha_5^{12} & & \\
\delta_5^{21} & \delta_5^{22} & \sigma_5^{21} & \sigma_5^{22} & \lambda_5^{21} & \lambda_5^{22} & \rho_5^{21} & \rho_5^{22} & \gamma_5^{21} & \gamma_5^{22} & \beta_5^{21} & \beta_5^{22} & \alpha_5^{21} & \alpha_5^{22} & & \\
 & \ddots & \ddots & \ddots & \ddots & \ddots & \ddots & \ddots & \ddots & \ddots & \ddots & \ddots & \ddots & \ddots & \ddots & \\
 & & \delta_n^{11} & \delta_n^{12} & \sigma_n^{11} & \sigma_n^{12} & \lambda_n^{11} & \lambda_n^{12} & \rho_n^{11} & \rho_n^{12} & \gamma_n^{11} & \gamma_n^{12} & \beta_n^{11} & \beta_n^{12} & \alpha_n^{11} & \alpha_n^{12} \\
 & & \delta_n^{21} & \delta_n^{22} & \sigma_n^{21} & \sigma_n^{22} & \lambda_n^{21} & \lambda_n^{22} & \rho_n^{21} & \rho_n^{22} & \gamma_n^{21} & \gamma_n^{22} & \beta_n^{21} & \beta_n^{22} & \alpha_n^{21} & \alpha_n^{22}
\end{pmatrix}
\begin{pmatrix} a_0^g \\ a_0^m \\ a_1^g \\ a_1^m \\ a_2^g \\ a_2^m \\ a_3^g \\ a_3^m \\ a_4^g \\ a_4^m \\ a_5^g \\ a_5^m \\ a_n^g \\ \vdots \\ a_n^m \end{pmatrix} = 0.$$

The QNFs are those that make the determinant of the coefficient matrix zero. This method was first used to solve the QNFs of the RN black holes by Leaver [75].

Except for the matrix-valued continued fraction method, we also use the matrix-valued direct integration method to solve the QNFs. More details can be seen in Ref. [77].

We solve the fundamental QNMs numerically, which dominate the ringdown waveform at late time. The values of the frequencies of fundamental QNMs for the gravitational field ψ_g and the magnetic field ψ_m for different values of the magnetic charge Q_m with $l = 2$ are shown in Tables I and II. When $Q_\mathrm{m} = 0$, the metric (15) reduces to the Schwarzschild metric. The master equation (37) reduces to the odd-parity gravitational perturbation of the Schwarzschild black hole in general relativity. The QNFs are also the same as the Schwarzschild black hole case. This confirms that our numerical method is valid. Besides, the QNFs solved by the matrix-valued direct integration method and the matrix-valued continued fraction method agree well each other, which can be seen in Tables I and II. This strengthens the validity of our results. Note that the charge of the charged black hole with scalar hair can be seen as a dark charge. One of the effects of this charge is to stabilize the spacetime. Besides, it is possible that microscopic topology stars could be candidates for dark matter. In this paper, we would like to compare our results with that of the RN black hole. Comparing the QNFs of the charged black hole with scalar hair and the RN black hole, we can see that the differences of their numerical values are very small. So we almost cannot

TABLE I. The fundamental QNMs for the gravitational field $\psi_{\rm g}$ of the charged black hole with scalar hair [using the direct integration (DI) method and using the continued fraction (CF) method] and the RN black hole for different values of the magnetic charge $Q_{\rm m}$ and electric charge Q, respectively. The angular number l is set to $l = 2$.

	Charged BH DI		Charged BH CF			RN BH	
$Q_{\rm m}/M$	$\omega_{\rm R}M$	$\omega_{\rm I}M$	$\omega_{\rm R}M$	$\omega_{\rm I}M$	Q/M	$\omega_{\rm R}M$	$\omega_{\rm I}M$
0	0.37367	−0.088962	0.37367	−0.088962	0	0.37367	−0.088962
0.2	0.37474	−0.089081	0.37480	−0.089095	0.2	0.37474	−0.089075
0.4	0.37848	−0.089429	0.37855	−0.089463	0.4	0.37844	−0.089398
0.6	0.38641	−0.089982	0.38649	−0.090086	0.6	0.38622	−0.089814
0.8	0.40163	−0.090500	0.40169	−0.090886	0.8	0.40122	−0.089643
1.12	0.47027	−0.084231	0.47153	−0.092731	0.9999	0.43134 [78]	−0.083460 [78]

TABLE II. The fundamental QNMs for the magnetic field $\psi_{\rm m}$ of the charged black hole with scalar hair [using the direct integration (DI) method and using the continued fraction (CF) method] and the electric field $\psi_{\rm e}$ of the RN black hole for different values of the magnetic charge $Q_{\rm m}$ and electric charge Q, respectively. The angular number l is set to $l = 2$.

	Charged BH DI		Charged BH CF			RN BH	
$Q_{\rm m}/M$	$\omega_{\rm R}M$	$\omega_{\rm I}M$	$\omega_{\rm R}M$	$\omega_{\rm I}M$	Q/M	$\omega_{\rm R}M$	$\omega_{\rm I}M$
0	0.45715	−0.094784	0.45715	−0.094784	0	0.45759	−0.095004
0.2	0.46295	−0.095377	0.46296	−0.095359	0.2	0.46297	−0.095373
0.4	0.47969	−0.096462	0.47969	−0.096441	0.4	0.47993	−0.096442
0.6	0.51053	−0.098155	0.51055	−0.098133	0.6	0.51201	−0.098017
0.8	0.56316	−0.10008	0.56320	−0.10002	0.8	0.57013	−0.099069
1.12	0.78258	−0.091135	0.79925	−0.098085	0.9999	0.70430 [78]	−0.085973 [78]

distinguish them from the gravitational wave data. Note that, for the extreme RN black hole, the singular structure of the perturbation equations is different from the non-extreme ones. The QNMs for the maximally charged RN black hole were studied in Ref. [78]. Our results for the RN black hole with $Q/M = 0.9999$ are taken from that paper. It is valuable to compare the QNFs of the nearly extremal charged black hole with that of the RN black hole. However, we can only calculate the QNFs for $Q_{\rm m}/M = 1.12$ or, equivalently, $Q_{\rm m}/M = 0.96995 \times (2/\sqrt{3})$. More extremal cases need special concern.

The effects of the magnetic charge $Q_{\rm m}$ of the charged black hole with scalar hair and the electric charge Q of the RN black hole on the fundamental QNMs are shown in Figs. 1 and 2. From Figs. 1(a) and 1(b), it can be seen that the real parts of the QNFs for both black holes increase with

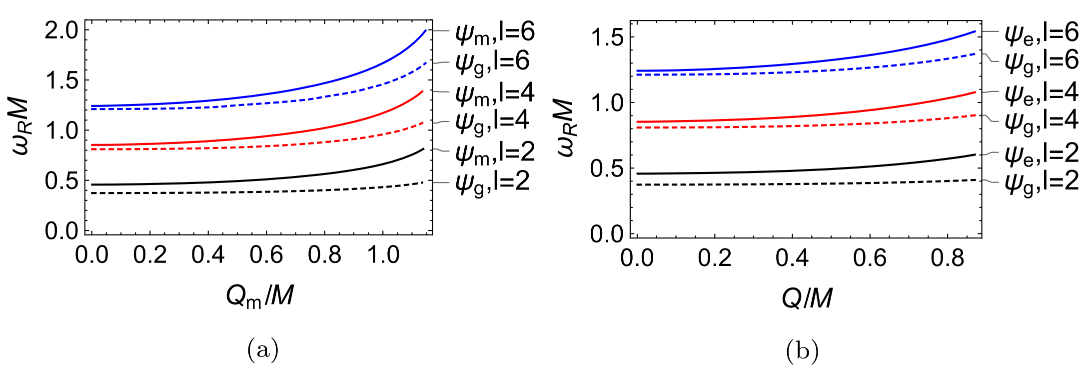

FIG. 1. The effects of the magnetic charge $Q_{\rm m}$ of the charged black hole with scalar hair and the electric charge Q of the RN black hole on the real parts of the fundamental QNFs. The solid and dashed lines correspond to the QNFs of the magnetic field $\psi_{\rm m}$ (or the electric field $\psi_{\rm e}$) and the gravitational field $\psi_{\rm g}$, respectively. The black, red, and blue lines correspond to the QNFs with $l = 2$, $l = 4$, and $l = 6$, respectively. (a) The real parts of the QNFs for the charged black hole with scalar hair. (b) The real parts of the QNFs for the RN black hole.

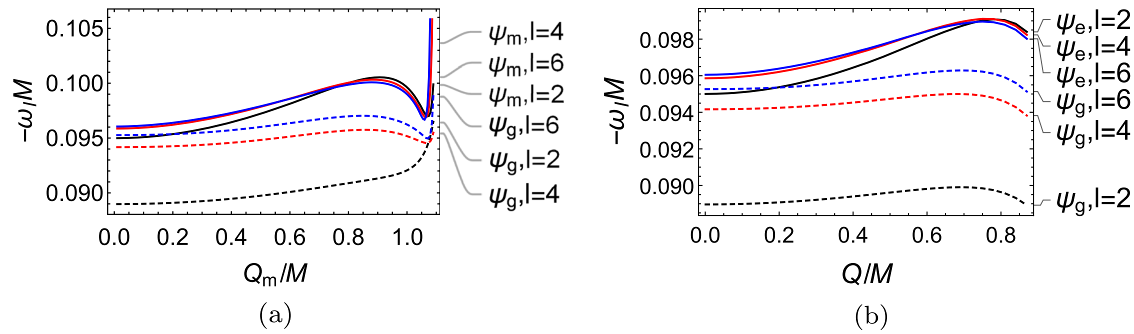

FIG. 2. The effects of the magnetic charge Q_m of the charged black hole with scalar hair and the electric charge Q of the RN black hole on the imaginary parts of the fundamental QNFs. The solid and dashed lines correspond to the QNFs of the magnetic field ψ_m (or the electric field ψ_e) and the gravitational field ψ_g, respectively. The black, red, and blue lines correspond to the QNFs with $l = 2$, $l = 4$, and $l = 6$, respectively. (a) The imaginary parts of the QNFs for the charged black hole with scalar hair. (b) The imaginary parts of the QNFs for the RN black hole.

the magnetic charge Q_m or the electric charge Q. The imaginary parts of the QNFs for the RN black hole first increase, then decrease as the electric charge Q increases, which can be seen in Fig. 2(b). However, the situation for the imaginary parts of the charged black hole with scalar hair is different, which can be seen in Fig. 2. The imaginary part for the gravitational field ψ_g of the charged black hole with scalar hair when $l = 2$ [the black dashed line in Fig. 2(a)] increases with the magnetic charge Q_m. The imaginary part for the gravitational field ψ_g when $l > 2$ and for the magnetic field ψ_m when $l \geq 2$ first increases, then decreases, and finally increases as the magnetic charge Q_m increases. We also calculate the QNFs for $l = 7, 8, 9$, and the results are shown in the Supplemental Material [79].

V. CONCLUSIONS

In five-dimensional spacetime, based on the Einstein-Maxwell action (1), Bah and Heidmann proposed a nonsingular black hole/topology star. This is similar to the classical black hole in macrostate geometries; more importantly, it can be constructed from type-IIB string theory. Integrating the extra dimension y, the five-dimensional Einstein-Maxwell theory reduces to a four-dimensional Einstein-Maxwell-dilaton theory, which supports a spherically static black hole/topological star solution with a magnetic charge.

We investigated the QNMs of the charged black hole with scalar hair by studying the linear perturbation of the gravitational field and the electromagnetic field. Because of the spherical symmetry of the background spacetime, the radial parts of the perturbed fields can be decomposed from the angular parts. The angular parts can be expanded by the spherical harmonics. The background scalar field (12) and metric field (15) are even parity under the space inversion; however, the background magnetic field (13) is odd parity. So the scalar perturbation and even-parity parts of the metric perturbations couple to the odd-parity parts of the electromagnetic perturbations to the linear order, and the odd-parity parts of the metric perturbations couple to the even-parity parts of the electromagnetic perturbations to the linear order, which we named as type-I and type-II couplings, respectively. For simplicity, we study the type-II coupling perturbations. Finally, we obtained two coupled perturbation equations (37) and (38). Although the extra dimension radius R_y can be eliminated from the master equations by a transformation of the electromagnetic field ψ_m, it can also affect the QNM spectrum through the gravitational constant.

Using the matrix-valued direct integration method and the matrix-valued continued fraction method, we computed the fundamental QNFs for both the gravitational perturbation and the magnetic field perturbation, which will dominate the ringdown wave at late time. The values of the frequencies of the fundamental QNMs for the gravitational field ψ_g and the magnetic field ψ_m for different values of the magnetic charge Q_m with $l = 2$ are shown in Tables I and II. The results obtained from the matrix-valued direct integration method and the matrix-valued continued fraction method agree well each other, which strengthens the validity of our results. The differences of the frequencies of the fundamental QNMs between the charged black hole with scalar hair and the RN black hole are very small. So we almost cannot distinguish them from the gravitational wave data. The effect of the magnetic charge Q_m of the charged black hole with scalar hair on the fundamental QNFs are shown in Figs. 1(a) and 2. The real parts of the QNFs increase with the magnetic charge Q_m, which is similar to that of the RN black hole. However, the situation for the imaginary parts of the QNFs of the charged black hole with scalar hair is different, which can be seen in Fig. 2.

We only studied the type-II coupling perturbations, where the scalar field does not couple to the other two fields. So we expect that the type-I coupling perturbations will give us more information about the charged black hole with scalar hair, which will be studied in the future.

ACKNOWLEDGMENTS

We thank Pierre Heidmann for important comments, suggestions, and discussion. W.-D. G. and Q. T. are co-first authors of this paper. This work was supported by National Key Research and Development Program of China (Grant No. 2020YFC2201503), the National Natural Science Foundation of China (Grants No. 12205129, No. 12147166, No. 11875151, No. 12075103, and No. 12247101), the China Postdoctoral Science Foundation (Grant No. 2021M701529), the 111 Project (Grant No. B20063), and Lanzhou City's scientific research funding subsidy to Lanzhou University.

APPENDIX: EXPLICIT PERTURBATION EQUATIONS

In this appendix we give the details for how to get the master perturbation equations (37) and (38). The nonvanishing parts of the perturbed Einstein equations are the (t,ϕ), (r,ϕ), and (θ,ϕ) components

$$2e\left(4f_B\frac{r_S}{r}-f_S\frac{r_B}{r}-\frac{f_S r_B^2}{f_B r^2}+4l(l+1)+10f_S\frac{r_B}{r}+8\frac{r_S}{r}+12\frac{r_B r_S}{r^2}\right)h_0-8ef_Bf_Sr^2h_0'' \\ -4ief_Sr\omega(rf_B'+4f_B)h_1-8ief_Bf_Sr^2\omega h_1'=-16a\sqrt{G_4}\sqrt{f_B}f_{02}, \tag{A1}$$

$$8ef_B^2(r^4\omega^2-f_S(r_S(2f_B+3r_B)-2rf_Br_S+(l(l+1)-2)r^2))h_1+4i\frac{e}{r}f_B\omega(4f_B+rf_B')h_0 \\ -8ier^4f_B^2\omega h_0'=16a\sqrt{G_4}r^2f_B^{5/2}f_Sf_{12}, \tag{A2}$$

$$2f_Sh_1f_Bf_S'+f_S^2(h_1f_B'+2f_Bh_1')+2ih_0\omega=0, \tag{A3}$$

where the constant a is defined as $a\equiv e\sqrt{3r_Br_S}$. And the nonvanishing parts of the perturbed Maxwell equations are the t, r, and θ components

$$f_Sr(rf_B'+4f_B)f_{01}+2f_Bf_Sr^2f_{01}'-2l(l+1)f_{02}=\frac{a}{f_Br^2\sqrt{G_4}}l(l+1)h_0, \tag{A4}$$

$$2i\omega\sqrt{f_B}r^4f_{01}+2f_S\sqrt{f_B}r^2l(l+1)f_{12}=-\frac{a}{\sqrt{G_4}}f_Sl(l+1)h_1, \tag{A5}$$

$$2f_B^{3/2}f_S\kappa_4r^3(f_{12}f_S)'+\sqrt{f_B}r^3(f_{12}f_S^2f_B'+2if_{02}\omega)=\frac{a}{\sqrt{G_4}}(3f_Sh_1-f_Bf_S(f_Srh_1)'-\omega rh_0). \tag{A6}$$

Actually, among the six perturbed equations only four of them are independent. Equation (A1) can be derived from Eqs. (A2), (A3), and (A6) with the background Einstein equation (9). Similarly, Eq. (A6) can also be obtained by using Eqs. (A5) and (A4). Therefore, we can use four independent equations (A2)–(A5) and an identity (36) to solve five independent variables h_0, h_1, f_{01}, f_{02}, and f_{12}.

The variable h_0 can be solved from Eq. (A3) as

$$h_0=\frac{i}{2\omega}f_S(f_Sf_B'+2f_Bf_S')h_1+2f_S^2f_Bh_1'. \tag{A7}$$

Using this formula and Eqs. (A4) and (A5), we can obtain f_{02} and f_{12} in terms of h_1 and f_{01} as

$$f_{02}=\frac{f_Sr}{2l(l+1)}[2rf_Bf_{01}'+(4f_B+rf_B')f_{01}]-\frac{iaf_S}{4r^2\sqrt{G_4}\omega\sqrt{f_B}}[2f_B(h_1f_S)'+f_Sf_B'h_1], \tag{A8}$$

$$f_{12}=-\frac{i\omega r^2}{f_S(l+1)l}f_{01}-\frac{a}{2\sqrt{G_4}\sqrt{f_B}r^2}h_1. \tag{A9}$$

Substituting Eqs. (A7)–(A9) into Eqs. (A2) and (36) we can obtain two second-order differential equations in which h_1 and f_{01} are coupled

$$-\frac{1}{2}\sqrt{f_B}f_S h_1'' + \left[\frac{\sqrt{f_B}}{2r^2}(2rf_S - 3r_S) - \frac{r_B f_S}{2r^2\sqrt{f_B}}\right]h_1' + \left[\frac{r_B^2 f_S}{8r^4 f_B^{3/2}} - \frac{\omega^2}{2\sqrt{f_B}f_S} - \frac{1}{4r^4\sqrt{f_B}}((3r_B r_S - 2(l-1)(l+2)r^2) - 5rr_B f_S) + \frac{\sqrt{f_B}}{2r^4 f_S}(4rr_S f_S - r_S^2)\right]h_1 = \frac{2i\omega a\sqrt{G_4}}{e^2 l(l+1)f_S}f_{01}, \tag{A10}$$

$$-\frac{r^2 f_S f_B}{l(l+1)}f_{01}'' + \frac{2f_B(r_S + 4rf_S) - 3r_B f_S}{2l(l+1)}f_{01}' + \left[1 - \frac{r^2\omega^2}{l(l+1)f_S} + \frac{f_S'(4rf_B + r_B)}{2l(l+1)} - \frac{f_S(5r_B + 4rf_B f_S)}{2l(l+1)r}\right]f_{01}$$
$$= -\frac{ia\sqrt{f_B}f_S^2}{2r^2\omega\sqrt{G_4}}h_1'' - \frac{iaf_S[r_B f_S + f_B(3r_S - 2rf_S)]}{2r^4\omega\sqrt{G_4}f_B}h_1' - \frac{iar_B^2 f_S^2}{8r^6\omega\sqrt{G_4}f_B^{3/2}}h_1 + \left[\frac{iar_S\sqrt{f_B}(r_S - 3rf_S)}{2r^6\omega\sqrt{G_4}} - \frac{ia(3rr_B f_S^2 - 2r^4\omega^2 - 3r_B r_S f_S)}{4r^6\omega\sqrt{G_4}\sqrt{f_B}}\right]h_1. \tag{A11}$$

To get the Schrödinger-like form, we need to define the following master variables:

$$\psi_{\mathrm{g}} \equiv f_B^{1/4} f_S \frac{1}{r} h_1, \tag{A12}$$

$$\psi_{\mathrm{m}} \equiv \sqrt{f_B} r^2 f_{01}. \tag{A13}$$

In the tortoise coordinate r_*, Eqs. (A10) and (A11) can be rewritten into the form of Eqs. (37) and (38).

[1] LIGO Collaboration and Virgo Collaboration, Observation of Gravitational Waves from a Binary Black Hole Merger, Phys. Rev. Lett. **116**, 061102 (2016).

[2] EHT Collaboration, First M87 event horizon telescope results. I. The shadow of the supermassive black hole, Astrophys. J. Lett. **875**, L1 (2019).

[3] EHT Collaboration, First M87 event horizon telescope results. II. Array and instrumentation, Astrophys. J. Lett. **875**, L2 (2019).

[4] EHT Collaboration, First M87 event horizon telescope results. III. Data processing and calibration, Astrophys. J. Lett. **875**, L3 (2019).

[5] EHT Collaboration, First M87 event horizon telescope results. IV. Imaging the central supermassive black hole, Astrophys. J. Lett. **875**, L4 (2019).

[6] EHT Collaboration, First M87 event horizon telescope results. V. Physical origin of the asymmetric ring, Astrophys. J. Lett. **875**, L5 (2019).

[7] EHT Collaboration, First M87 event horizon telescope results. VI. The shadow and mass of the central black hole, Astrophys. J. Lett. **875**, L6 (2019).

[8] EHT Collaboration, First sagittarius A* event horizon telescope results. I. The shadow of the supermassive black hole in the center of the Milky Way, Astrophys. J. Lett. **930**, L12 (2022).

[9] EHT Collaboration, First sagittarius A* event horizon telescope results. II. EHT and multiwavelength observations, data processing, and calibration, Astrophys. J. Lett. **930**, L13 (2022).

[10] EHT Collaboration, First sagittarius A* event horizon telescope results. III. Imaging of the galactic center supermassive black hole, Astrophys. J. Lett. **930**, L14 (2022).

[11] EHT Collaboration, First sagittarius A* event horizon telescope results. IV. Variability, morphology, and black hole mass, Astrophys. J. Lett. **930**, L15 (2022).

[12] EHT Collaboration, First sagittarius A* event horizon telescope results. V. Testing astrophysical models of the Galactic center black hole, Astrophys. J. Lett. **930**, L16 (2022).

[13] EHT Collaboration, First sagittarius A* event horizon telescope results. VI. Testing the black hole metric, Astrophys. J. Lett. **930**, L17 (2022).

[14] E. Berti, E. Barausse, V. Cardoso, L. Gualtieri, P. Pani, U. Sperhake *et al.*, Testing general relativity with present and future astrophysical observations, Classical Quantum Gravity **32**, 243001 (2015).

[15] V. Cardoso, E. Franzin, and P. Pani, Is the Gravitational-Wave Ringdown a Probe of the Event Horizon?, Phys. Rev. Lett. **116**, 171101 (2016).

[16] P. O. Mazur and E. Mottola, Gravitational condensate stars: An alternative to black holes, Universe **9**, 88 (2023).

[17] F. E. Schunck and E. W. Mielke, Topical review: General relativistic boson stars, Classical Quantum Gravity **20**, R301 (2003),

[18] S. N. Solodukhin, Restoring unitarity in BTZ black hole, Phys. Rev. D **71**, 064006 (2005).

[19] D.-C. Dai and D. Stojkovic, Observing a wormhole, Phys. Rev. D **100**, 083513 (2019).

[20] J. H. Simonetti, M. J. Kavic, D. Minic, D. Stojkovic, and D.-C. Da, Sensitive searches for wormholes, Phys. Rev. D **104**, L081502 (2021).

[21] C. Bambi and D. Stojkovic, Astrophysical wormholes, Universe **7**, 136 (2021).

[22] V. Cardoso and P. Pani, Testing the nature of dark compact objects: A status report, Living Rev. Relativity **22**, 4 (2019).

[23] G. W. Gibbons and N. P. Warner, Global structure of five-dimensional BPS fuzzballs, Classical Quantum Gravity **31**, 025016 (2014),

[24] I. Bena, F. Eperon, P. Heidmann, and N. P. Warner, The great escape: Tunneling out of microstate geometries, J. High Energy Phys. 04 (2021) 112.

[25] I. Bena and D. R. Mayerson, A New Window into Black Holes, Phys. Rev. Lett. **125**, 221602 (2020).

[26] I. Bena and D. R. Mayerson, Black holes lessons from multipole ratios, J. High Energy Phys. 03 (2021) 114.

[27] I. Bah and P. Heidmann, Topological Stars and Black Holes, Phys. Rev. Lett. **126**, 151101 (2021).

[28] I. Bah and P. Heidmann, Topological stars, black holes and generalized charged weyl solutions, J. High Energy Phys. 09 (2021) 147.

[29] Y.-K. Lim, Motion of charged particles around a magnetic black hole/topological star with a compact extra dimension, Phys. Rev. D **103**, 084044 (2021).

[30] I. Bah, A. Dey, and P. Heidmann, Stability of topological solitons, and black string to bubble transition, J. High Energy Phys. 04 (2022) 168.

[31] W.-D. Guo, S.-W. Wei, and Y.-X. Liu, Shadow of a nonsingular black hole, Eur. Phys. J. C **83**, 197 (2023).

[32] E. Berti, V. Cardoso, J. A. Gonzalez, and U. Sperhake, Mining information from binary black hole mergers: A comparison of estimation methods for complex exponentials in noise, Phys. Rev. D **75**, 124017 (2007).

[33] H. P. Nollert and R. H. Price, Quantifying excitations of quasinormal mode systems, J. Math. Phys. (N.Y.) **40**, 980 (1999).

[34] F. Echeverria, Gravitational wave measurements of the mass and angular momentum of a black hole, Phys. Rev. D **40**, 3194 (1989).

[35] E. Berti, V. Cardoso, and C. M. Will, On gravitational-wave spectroscopy of massive black holes with the space interferometer LISA, Phys. Rev. D **73**, 064030 (2006).

[36] E. Berti, J. Cardoso, V. Cardoso, and M. Cavaglia, Matched-filtering and parameter estimation of ringdown waveforms, Phys. Rev. D **76**, 104044 (2007).

[37] M. Isi, M. Giesler, W. M. Farr, M. A. Scheel, and S. A. Teukolsky, Testing the No-Hair Theorem with GW150914, Phys. Rev. Lett. **123**, 111102 (2019).

[38] V. Cardoso and P. Pani, Tests for the existence of black holes through gravitational wave echoes, Nat. Astron. **1**, 586 (2017).

[39] J. Jaramillo, R. P. Macedo, and L, A. Sheikh, Pseudospectrum and Black Hole Quasinormal Mode Instability, Phys. Rev. X **11**, 031003 (2021).

[40] M. H. Cheung, K. Destounis, R. P. Macedo, E. Berti, and V. Cardoso, Destabilizing the Fundamental Mode of Black Holes: The Elephant and the Flea, Phys. Rev. Lett. **128**, 111103 (2022).

[41] B. Wang, C.-Y. Lin, and C. Molina, Quasinormal behavior of massless scalar field perturbation in Reissner-Nordström anti-de Sitter spacetimes, Phys. Rev. D **70**, 064025 (2004).

[42] J. L. Blázquez-Salcedo, C. F. B. Macedo, V. Cardoso, V. Ferrari, and L. Gualtieri, Perturbed black holes in Einstein-dilaton-Gauss-Bonnet gravity: Stability, ringdown, and gravitational-wave emission, Phys. Rev. D **94**, 104024 (2016).

[43] G. Franciolini, L. Hui, R. Penco, L. Santoni, and E. Trincherini, Effective field theory of black hole quasinormal modes in scalar-tensor theories, J. High Energy Phys. 02 (2019) 127.

[44] A. Aragón, P. A. González, E. Papantonopoulos, V. Ferrari, and Y. Vásquez, Quasinormal modes and their anomalous behavior for black holes in $f(R)$ gravity, Eur. Phys. J. C **81**, 407 (2021).

[45] H. Liu, P. Liu, Y.-Q. Liu, B. Wang, and J.-P. Wu, Echoes from phantom wormholes, Phys. Rev. D **103**, 024006 (2021).

[46] T. Karakasis, E. Papantonopoulos, and C. Vlachos, f(R) gravity wormholes sourced by a phantom scalar field, Phys. Rev. D **105**, 024006 (2022).

[47] P. A. Cano, K. Fransen, T. Hertog, and S. Maenaut, Gravitational ringing of rotating black holes in higher-derivative gravity, Phys. Rev. D **105**, 024064 (2022).

[48] P. A. González, E. Papantonopoulos, J. Saavedra, and Y. Vásquez, Quasinormal modes for massive charged scalar fields in Reissner-Nordström dS black holes: Anomalous decay rate, J. High Energy Phys. 06 (2022) 150.

[49] Y. Zhao, R. Xin, A. Ilyas, E. N. Saridakis, and Y.-F. Cai, Quasinormal modes of black holes in $f(T)$ gravity, J. Cosmol. Astropart. Phys. 10 (2022) 087.

[50] A. Ishibashi and H. Kodama, Stability of higher dimensional Schwarzschild black holes, Prog. Theor. Phys **110**, 901 (2003).

[51] A. Chowdhury, S. Devi, and S. Chakrabarti, Naked singularity in 4D Einstein-Gauss-Bonnet novel gravity: Echoes and (in)-stability, Phys. Rev. D **106**, 024023 (2022).

[52] K. Kristensen, R.-C. Ge, and S. Hughes, Normalization of quasinormal modes in leaky optical cavities and plasmonic resonators, Phys. Rev. A **92**, 053810 (2015).

[53] S. S. Seahra, Ringing the Randall-Sundrum braneworld: Metastable gravity wave bound states, Phys. Rev. D **72**, 066002 (2005).

[54] S. S. Seahra, Metastable massive gravitons from an infinite extra dimension, Int. J. Mod. Phys. D **14**, 2279 (2005).

[55] Q. Tan, W.-D. Guo, and Y.-X. Liu, Sound from extra dimension: Quasinormal modes of thick brane, Phys. Rev. D **106**, 044038 (2022).

[56] Y.-F. Cai, G. Cheng, J. Liu, M. Wang, and H. Zhang, Features and stability analysis of non-Schwarzschild black hole in quadratic gravity, J. High Energy Phys. 01 (2016) 108.

[57] V. Cardoso, M. Kimura, A. Maselli, E. Berti, and C. F. B. Macedo, Parametrized black hole quasinormal ringdown:

Decoupled equations for nonrotating black holes, Phys. Rev. D **99**, 104077 (2019).

[58] R. McManus, E. Berti, C. F. B. Macedo, M. Kimura, A. Maselli, and V. Cardoso, Parametrized black hole quasinormal ringdown. II. Coupled equations and quadratic corrections for nonrotating black holes, Phys. Rev. D **100**, 044061 (2019).

[59] V. Cardoso, W.-D. Guo, C. F. B. Macedo, and P. Pani, The tune of the Universe: The role of plasma in tests of strong-field gravity, Mon. Not. R. Astron. Soc. **503**, 563 (2021).

[60] G. Guo, P. Wang, H. Wu, and H. Yang, Quasinormal modes of black holes with multiple photon spheres, J. High Energy Phys. 06 (2022) 060.

[61] S. Stotyn and R. B. Mann, Magnetic charge can locally stabilize kaluza-klein bubbles, Phys. Lett. B **705**, 269 (2011).

[62] R. Gregory and R. Laflamme, Black Strings and p-Branes are Unstable, Phys. Rev. Lett. **70**, 2837 (1993).

[63] J. A. Wheeler, *Geometrodynamics* (Academic Press, New York, 1973).

[64] A. R. Ruffini, *Black Holes: les Astres Occlus* (Gordon and Breach Science Publishers, New York, 1973).

[65] A. R. Ruffini, *Angular Momentum in Quantum Mechanics* (Princeton University Press, Princeton, NJ, 1996).

[66] T. Regge and J. A. Wheeler, Stability of a Schwarzschild singularity, Phys. Rev. **108**, 1063 (1957).

[67] S. Chandrasekhar, *The Mathematical Theory of Black Holes* (Oxford University Press, New York, 1983).

[68] K. Nomura, D. Yoshida, and J. Soda, Stability of magnetic black holes in general nonlinear electrodynamics, Phys. Rev. D **101**, 124026 (2020).

[69] K. Meng and S.-J. Zhang, Gravito-electromagnetic perturbations and QNMs of regular black holes, arXiv:2210.00295.

[70] F. J. Zerilli, Perturbation analysis for gravitational and electromagnetic radiation in a Reissner-Nordström geometry, Phys. Rev. D **9**, 860 (1974).

[71] E. W. Leaver, An analytic representation for the quasinormal modes of Kerr black holes, Proc. R. Soc. A **402**, 285 (1985).

[72] C. Simmendinger, A. Wunderlin, and A. Pelster, Analytical approach for the Floquet theory of delay differential equations, Phys. Rev. E **59**, 5344 (1999).

[73] J. G. Rosa and S. R. Dolan, Massive vector fields on the Schwarzschild spacetime: Quasi-normal modes and bound states, Phys. Rev. D **85**, 044043 (2012).

[74] If you want the explicit expressions of the recurrence relations, please contact Wen-Di Guo through guowd@lzu.edu.cn.

[75] E. W. Leaver, Quasinormal modes of Reissner-Nordström black holes, Phys. Rev. D **41**, 2986 (1990).

[76] E. Berti, S. Cardoso, and A. O. Starinets, Quasinormal modes of black holes and black branes, Classical Quantum Gravity **26**, 163001 (2009).

[77] P. Pani, Advanced methods in black-hole perturbation theory, Int. J. Mod. Phys. A **28**, 1340018 (2013).

[78] H. Onozawa, T. Mishima, T. Okamura, and H. Ishihara, Quasinormal modes of maximally charged black holes, Phys. Rev. D **53**, 7033 (1996).

[79] See Supplemental Material at http://link.aps.org/supplemental/10.1103/PhysRevD.107.124046 for the effects of the magnetic charge Q_m of the charged black hole with scalar hair on the fundamental QNFs for $l = 7, 8, 9$.